Accepted Manuscript

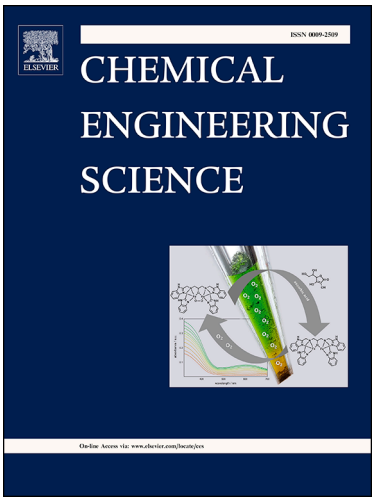

Modelling Reaction and Diffusion in a Wax-Filled Hollow Cylindrical Pellet of Fischer Tropsch Catalyst

R. Hubble, A.P.E. York, J.S. Dennis

PII: S0009-2509(19)30554-8
DOI: https://doi.org/10.1016/j.ces.2019.06.051
Reference: CES 15072

To appear in: *Chemical Engineering Science*

Received Date: 3 April 2019
Revised Date: 16 June 2019
Accepted Date: 29 June 2019

Please cite this article as: R. Hubble, A.P.E. York, J.S. Dennis, Modelling Reaction and Diffusion in a Wax-Filled Hollow Cylindrical Pellet of Fischer Tropsch Catalyst, *Chemical Engineering Science* (2019), doi: https://doi.org/10.1016/j.ces.2019.06.051

Modelling Reaction and Diffusion in a Wax-Filled Hollow Cylindrical Pellet of Fischer Tropsch Catalyst

R. Hubble[1], A.P.E. York[2], J. S. Dennis[1*]

[1] Department of Chemical Engineering & Biotechnology, University of Cambridge, Philippa Fawcett Drive, Cambridge, CB3 0AS, United Kingdom,
[2] Johnson Matthey Technology Centre, Blounts Court Road, Sonning Common, Reading, RG4 9NH, United Kingdom
**Corresponding Author, email address: jsd3@cam.ac.uk*

Abstract

Previous modelling of fixed-bed, Fischer-Tropsch (FT) reactors has demonstrated the advantages relative to spherical pellets of using cylindrical and shaped pellets to provide improved transport attributes under conditions relevant to industrial operation. However, mass transport models have focussed on the investigation of transport within pellets with spherical symmetry, whilst detailed investigations of more complex shapes have not been undertaken. Here, a pseudo-isothermal, steady-state, two-dimensional model was investigated for catalyst pellets of cylindrical form, both solid and hollow. A cobalt-based catalyst was considered at conditions where the rate of condensable hydrocarbon generation is large enough to result in the accumulation of liquid hydrocarbons in the pores of a catalyst. It was found that effectiveness factors were bounded by those of sphere and slab above and below Thiele moduli of ~0.75 and ~1.15, respectively, for the conditions examined, with the effectiveness factors exceeding those of both sphere and slab models between these moduli. Here, comparisons were made on the basis of the characteristic diffusion length, the catalyst particle's volume divided by its external surface area. However, values of the FT chain growth parameter, α, between these values of Thiele modulus were lower than both those of sphere and slab geometry, and thus under these conditions hollow cylinders gave the greatest methane selectivity.

1 Introduction

1.1 The Fischer-Tropsch Reaction

Synthesis gas, predominantly a mixture of carbon monoxide (CO) and hydrogen (H_2), can be transformed directly to linear alkanes and alkenes using the Fischer-Tropsch (FT) process. The main reaction pathways are summarised by equations (1) to (3), below. Equations (4) and (5) describe secondary reactions which may occur in parallel with the Fischer-Tropsch reactions, namely the water gas shift and Boudouard reactions.

$$CO + 3H_2 \leftrightarrow CH_4 + H_2O \quad (1)$$

$$nCO + 2nH_2 \leftrightarrow C_nH_{2n} + nH_2O \quad (2)$$

$$nCO + (2n+1)H_2 \leftrightarrow C_nH_{2n+2} + nH_2O \quad (3)$$

$$CO + H_2O \leftrightarrow CO_2 + H_2 \quad (4)$$

$$2CO \leftrightarrow C^* + CO_2 \quad (5)$$

Here, * indicates a species bound to the surface of the catalyst. From a thermodynamic standpoint, both methanation, reaction (1), and carbon deposition, reaction (5), are favourable compared to the formation of hydrocarbons, particularly at high temperatures (Snel, 1987). However, in practice, kinetic and mass transport factors dictate the observed activity and selectivity of the process (Snel, 1987), usually favouring hydrocarbon formation.

The Fischer-Tropsch process typically operates between 200°C and 340°C (Leckel, 2009) and at pressures $\geq$ 20 barg (Dry, 2002). Generally, an FT reactor will be operated in either a low-temperature (< 260°C) or a high-temperature (310-340°C) regime (Leckel, 2009). The choice of catalyst (with iron and cobalt employed on an industrial scale), temperature, pressure and CO/H_2 ratio all have an effect on the mean molecular weight of the products. The range of products obtained is often modelled with an Anderson-Schulz-Flory (ASF) distribution, which assumes that chain growth on the surface of the catalyst occurs only through the addition of a single monomer unit containing one carbon atom, with termination taking place *via* chain desorption (Novak *et al.*, 1981). Hence:

$$W_N = N(1-\alpha)^2\alpha^{N-1} \quad (6)$$

where

$$\alpha = \frac{k_p}{k_p + k_t} \quad (7)$$

Here, W_N is the weight fraction of product of carbon number N and α is the chain growth parameter. The rate constants k_p and k_t are, respectively, for chain propagation and chain termination. The chain growth parameter, α, describes the likelihood of chain growth and can

be determined from the gradient of an ASF plot of $\log(W_N/N)$ against , N. This single-parameter model can provide a reasonable fit to experimental results; however, it assumes that the chain growth parameter is independent of carbon number (Novak *et al.*, 1981). In modelling, the α parameter is significant, since it is necessary to determine the ratio of the rates of CO and H_2 consumption as well as the product composition. The parameter is notably sensitive to pressure, temperature and the local ratio of H_2 to CO. Experimentally, a product distribution may deviate from a single α distribution at higher carbon numbers, with the ASF plot showing changes in gradient corresponding, *e.g.* to their being two or more distinct values of α. Various reasons for such deviations have been proposed, including the existence of two different reaction sites (Huff and Satterfield, 1984), alkene readsorption and reincorporation (Iglesia *et al.*, 1991), secondary reactions due to increased physisorption of larger chains (Kuipers *et al.*, 1996), coincident reaction *via* the carbide and CO insertion mechanisms (Gaube and Klein, 2008) and the influence of vapour-liquid equilibrium (Masuku *et al.,* 2011).

1.2 Modelling the Reaction in Catalyst Pellets

The modelling of transport mechanisms and reaction kinetics in pellets of Fischer-Tropsch catalysts enables the effectiveness factor and the variation of the ratio of CO to H_2 across the radius of a catalyst particle to be ascertained. The former indicates whether the catalytic metal is being used optimally, whilst variations in the ratio of CO to H_2 affect the chain growth parameter, with high intra-pellet ratios of H_2 to CO causing excessive and undesired methane production. The Fischer-Tropsch process is known to suffer from intra-particle transport limitations in industrially-sized pellets of millimetre scale, with smaller particles deemed unsuitable due to excessive fixed-bed pressure drops. Current fixed-bed reactor simulations have highlighted the advantages relative to spherical pellets of using cylindrical and shaped pellets to provide improved hydrodynamic, heat and mass transport attributes under industrial conditions. However, mass transport models have focussed on the investigation of transport within pellets with spherical, or other 1-D, symmetry, whilst detailed investigations of more complex shapes have not been undertaken.

1.2.1 Intra-Particle Reaction-Diffusion Modelling

Evidence of internal diffusion limitation within Fischer-Tropsch pellets was first presented by Anderson *et al.* (1952). Later, Post *et al.* (1989) quantified the effect of pellet and pore diameter on reaction rate using a Thiele modulus approach with the kinetics simplified to a first-order reaction dependent on the partial pressure of hydrogen. In fitting this model to experiments, the calculated hydrogen diffusivity was significantly lower than would be expected for gas

phase diffusion, leading to the conclusion that the mass transfer within low-temperature, Fischer-Tropsch catalyst pellets is controlled by the diffusivity of reacting species through a medium of hydrocarbon liquid.

Iglesia *et al.* (1991) postulated that the gradients introduced by diffusion affected the selectivity of the reaction for alkenes. Specifically, it was thought that the presence of a heavy paraffin liquid phase increased pore residence times and thus secondary reactions of 1-alkenes. The suggestion was that 1-alkene products were reincorporated into chain growth, and thus produced a heavier and more paraffinic product. Higher chain lengths have been further associated with increased physisorption of alkenes on pore walls, and increased retention within the pores (Kuipers *et al.*, 1995).

Numerical models of greater complexity than that of Post *et al.* (1989) were later developed. The key benefits of these models were the use of representative kinetic descriptions, simulation of both hydrogen and carbon monoxide concentrations and the ability to encompass selectivity within the kinetics. Wang *et al.* (2001), for example, simulated a spherical catalyst particle filled with a 'liquid wax', employing kinetic equations including their own alkene readsorption kinetic model. The authors used this model to analyse the performance of iron FT catalyst spheres, ~1-3 mm diameter, obtaining conclusions broadly aligned with those of Post *et al.* (1989). That is, the overall effectiveness factor decreased as the pellet diameter increased above a few hundred microns. Vervloet *et al.* (2012) developed a reaction-diffusion model for a cobalt catalyst particle. Similar to Wang *et al.* (2001), a chain growth parameter model, dependent on the local H_2/CO ratio, was used to calculate the overall product distribution, and thus simulate shifts in the Fischer-Tropsch product distribution due to internal mass transfer limitations. Gardezi and Joseph (2015) modelled the performance of egg-shell cobalt silica FT catalysts and concluded that such distributions afforded more efficient metal usage over conventional configurations of catalyst and might allow for the use of larger particles, thus reducing the pressure drop across a fixed bed reactor. Becker *et al.* (2014, 2016) examined the introduction of wide, transport pores aimed at improving mass transport, promoting C_{5+} selectivity and increasing effectiveness factor. The resulting numerical model was based on a micro-structured reactor of slab geometry with a catalyst coated channel wall, with the kinetics derived from the work of Yates and Satterfield (1991). The transport pores were considered to be unreactive, uniformly distributed within the wall, and with a lower tortuosity than the reactive pores. The catalyst was then optimised for transport pore fraction, with significant increases being predicted for the activity and selectivity for C_{5+} hydrocarbons.

The underlying bases of these numerical studies are limited to simple spherical catalyst

particles, allowing the transport equations to be reduced to a one-dimensional, two-point boundary value problem, thus significantly reducing the computational requirements to solve the system. Industrially, catalyst pellets are formed into various shapes and configurations; hence the simulation of higher dimensional pellets is required to give an insight into how the behaviour of these pellets compares to the simplified models.

1.2.2 Pellets of Cylindrical Geometry

Kaiser *et al.* (2014) compared powdered and cylindrical (1.5 mm diameter, 5 mm length) Co/TiO_2 catalyst pellets. In experimental measurements, there were significant differences in the selectivity and apparent effectiveness factor between the catalyst in pellet and ground form. To explain their findings, the authors used a simplified analytical model for effectiveness factor for reaction-diffusion within a slab, obtaining a reasonable agreement between experiment and theory. However, they noted that a more detailed numerical simulation would be required to achieve a more accurate solution. Brunner *et al.* (2015) employed a one-dimensional reactor model to examine the effect of pellet size and geometry on the performance of a wall cooled multi-tubular Fischer-Tropsch reactor. Both the size and shape of pellets were considered, but based on an effective diameter model, where the effective diameter was calculated for a sphere of equivalent volume, with the effectiveness factor calculated assuming a first order reaction. Nanduri and Mills (2015) developed a one-dimensional fixed bed model with a '2D' model of the catalyst particles in spherical and cylindrical geometry for an iron-based Fischer-Tropsch catalyst. The authors' model examined the pellet in 2D by considering a radial plane which could not be reduced to a single dimension. This was due to the lack of rotational symmetry owing to the presence of multiple holes. In their 2D catalyst scale modelling approach, the influence of axial contributions on pellet-scale diffusion however was not simulated.

The present paper presents the derivation and evaluation of a pseudo-isothermal, steady-state, two-dimensional model for catalyst pellets of cylindrical form, both solid and hollow. A cobalt-based catalyst was considered, normally used in low-temperature Fischer-Tropsch reactions, where the rate of condensable hydrocarbon generation is large enough to result in the accumulation of liquid hydrocarbons in the pores of a catalyst.

2 Model Development

For a cylindrical pellet, the problem must be considered as being two-dimensional to allow for diffusion in both the radial and axial directions.

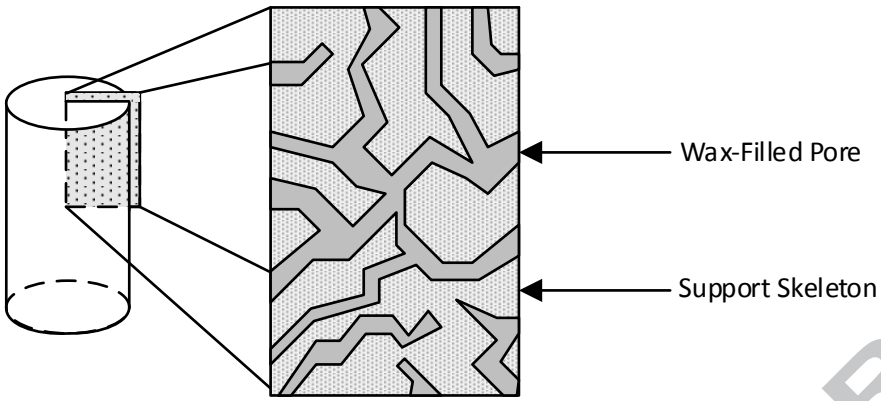

Figure 1. A schematic diagram of a liquid-filled Fischer-Tropsch catalyst pellet.

2.1 Assumptions

In modelling a liquid-filled Fischer-Tropsch pellet, schematically represented in Figure 1, the liquid-filled pores and the support skeleton were considered isotropic across the pellet. Diffusivities and thermal conductivities were calculated to account for both the structural parameters of the particle, *viz.* voidage, tortuosity, skeletal density and thermal conductivity, and the transport properties of the liquid in the pores. It was assumed that the reaction is at steady state, with the pores fully filled with liquid wax. The assumption of wax-filled pores has been noted to reflect the process behaviour by Wang *et al.* (2001), Madon and Iglesia (1994), and Huff and Satterfield (1985). In their study of pore-filling during reactor start-up, Huff and Satterfield (1985) reported that the time scale for pore filling depended significantly on the chain growth parameter and the activity of the catalyst, varying between about 2 and 90 hours for their fixed bed model. Huff and Satterfield (1985) assumed that reactant and product mass transport within the pores could be ignored, with the vapour-liquid equilibrium (VLE) determined by Raoult's law. Despite the simplicity of their model, the pore filling times were of similar order to those determined by Madon and Iglesia (1994), who compared 110-180 µm and 850-1700 µm diameter Ru/TiO_2 catalyst experimentally for Fischer-Tropsch synthesis (489 K, 505 kPa, H_2/CO_=_2). The larger particles were noted to display lower activity, and reached steady state within 20 hours. The smaller particles, however, reached steady state more rapidly, with less loss of activity. The behaviour of the larger particles was attributed to the mass transport influence introduced by pore filling, with the attainment of steady state attributed to the complete filling of the pores.

Here, the mass transport of dissolved CO and H_2 within the Fischer-Tropsch wax within the liquid-filled pores was described with Fick's law, as done by others, *e.g.* Wang *et al.* (2001), Gardezi and Joseph (2015), Vervloet *et al.* (2012). The use of Fick diffusion has been

confirmed as suitable by molecular dynamic simulations, with the Fick and Maxwell-Stefan diffusivities differing little for dissolved gas mole fractions below 0.1 (Makrodimitri *et al.*, 2011, Sanchez-Lopez *et al.*, 2016). The solubility of the CO and H_2 species within the waxy products is sufficiently low for these species to be considered dilute in concentration. The diffusivities of the species within the wax were assumed to depend only on the mean molecular mass of the wax within the pores and the process temperature. The flux of reactants was assumed to be controlled by diffusion and the contribution of advection due to outflow of liquid products was assumed to be negligible. The concentrations of the species at the pellet boundary dissolved within the wax phase were assumed to be in equilibrium with those in the gas phase, as described by Henry's law.

The thermal conductivity was taken to be uniform and constant across the solid pellet, with the influence of convection and radiation neglected. The influence of external heat transport was neglected and the pellet temperature boundary was assumed to be equal to the bulk temperature of the process fluid. The temperature gradients within the particle were found to be negligible for the conditions considered (< 0.2 K) and thus the pellet was assumed to be isothermal to improve simulation speed. This was checked by taking a system solved isothermally and using the reaction rates at each of the nodes to compute the rate of heat generation and ascertaining that the resulting gradients in temperature were small.

2.2 Mathematical Description

The generalised species transport equation at steady state may be expressed as

$$-\nabla\cdot\left(D_i\,\nabla\cdot\,C_i\right)-R_i=0 \tag{8}$$

where R_i is the reaction rate on a volumetric basis [mol/m^3 s], C_i the concentration [mol/m^3], and D_i [m^2/s] the effective diffusivity of species *i*. Likewise, the steady state temperature (T) gradients were expressed by equation (9). The molar heat of formation of species *j*, ΔH_j, and the rate of formation of species *j*, R_j, were summed over all species to calculate the overall heat of reaction, thus acting as the source term in the energy equation. The thermal conductivity, k, was a spatially-averaged combination of the thermal conductivities of the skeletal network of the support and the wax filling the pores.

$$-\nabla\cdot\left(k\,\nabla\cdot\,T\right)-\sum\Delta H_j R_j=0 \tag{9}$$

The following dimensionless variables were introduced.

$$\overline{C}_i = C_i/C_{i,0} \tag{10}$$

$$\overline{r} = r/r_p \tag{11}$$

$$\overline{z} = z/L \tag{12}$$

$$\overline{R}_i = R_i/R_{i,0} \tag{13}$$

$$\overline{T} = T/T_0 \tag{14}$$

Here barred quantities $\overline{C}_i$, $\overline{z}$, $\overline{T}$, $\overline{r}$, $\overline{R}$ represent the dimensionless concentration, axial position, temperature, radial position and reaction rate respectively, with *r* representing the radial position and *z* the axial position within the pellet. *L* is half the axial length and r_p is the radius of the pellet. The 0 subscripted terms represent the respective quantities at the outer surface of the pellet. Thus for a cylindrical system, equation (8) becomes

$$-\kappa_i\left(\frac{1}{\overline{r}}\frac{\partial}{\partial\overline{r}}\left(\overline{r}\frac{\partial\overline{C}_i}{\partial\overline{r}}\right)+\beta\left(\frac{\partial^2\overline{C}_i}{\partial\overline{z}^2}\right)\right)=\overline{R}_i \tag{15}$$

where $\kappa_i = \left(\frac{D_i C_{i,0}}{R_{i,0} {r_p}^2}\right)$ and $\beta = \frac{{r_p}^2}{L^2}$. For the evaluation and comparison of 1-D systems, the equations were reduced to (16)-(18).

Infinite Cylinder:
$$-\frac{DC_{i,0}}{R_{i,0}{r_p}^2}\left(\frac{1}{\overline{r}}\frac{\partial}{\partial\overline{r}}\left(\overline{r}\frac{\partial\overline{C}_i}{\partial\overline{r}}\right)\right)=\overline{R_i} \tag{16}$$

Sphere:
$$-\frac{DC_{i,0}}{R_{i,0}{r_p}^2}\left(\frac{1}{\overline{r}^2}\frac{\partial}{\partial\overline{r}}\left(\overline{r}^2\frac{\partial\overline{C}_i}{\partial\overline{r}}\right)\right)=\overline{R_i} \tag{17}$$

Slab:
$$-\frac{DC_{i,0}}{R_{i,0}L^2}\left(\frac{\partial^2\overline{C}_i}{\partial\overline{z}^2}\right)=\overline{R_i} \tag{18}$$

The energy equation (9) was expressed in non-dimensional form as

$$-\gamma\left(\frac{1}{\overline{r}}\frac{\partial}{\partial\overline{r}}\left(\overline{r}\frac{\partial\overline{T}}{\partial\overline{r}}\right)+\beta\left(\frac{\partial^2\overline{T}}{\partial\overline{z}^2}\right)\right)=\frac{\Delta H(r,z)}{\Delta H_0}\overline{R}_{CO} \tag{19}$$

Here, $\overline{R}_{CO} = \frac{R_{CO}}{R_{CO,0}}$ represents the local dimensionless reaction rate of CO and $\Delta H(r,z)$ the local heat of reaction per mole of CO at a given radius and axial co-ordinate, with the 0 subscript representing surface conditions. The dimensionless group $\gamma = \frac{kT_0}{\Delta H_0 R_{CO,0} {r_p}^2}$ is comprised of the

effective thermal conductivity, k, the surface temperature, T_0, the reaction enthalpy at the surface, ΔH_0, the reaction rate of CO at the surface, R_{CO}, and the pellet radius, r_p. For comparison with 1-D systems, the equations were reduced to (20)-(22).

Infinite Cylinder:
$$-\frac{kT_0}{\Delta H_0 R_{CO,0} {r_p}^2}\left(\frac{1}{\bar{r}}\frac{\partial}{\partial \bar{r}}\left(\bar{r}\frac{\partial \bar{T}}{\partial \bar{r}}\right)\right) = \frac{\Delta H(r)}{\Delta H_0}\bar{R}_{CO} \quad (20)$$

Sphere:
$$-\frac{kT_0}{\Delta H_0 R_{CO,0} {r_p}^2}\left(\frac{1}{\bar{r}^2}\frac{\partial}{\partial \bar{r}}\left(\bar{r}^2\frac{\partial \bar{T}}{\partial \bar{r}}\right)\right) = \frac{\Delta H(r)}{\Delta H_0}\bar{R}_{CO} \quad (21)$$

Slab:
$$-\frac{kT_0}{\Delta H R_{CO,0} L^2}\left(\frac{\partial^2 \bar{T}}{\partial \bar{z}^2}\right) = \frac{\Delta H(z)}{\Delta H_0}\bar{R}_{CO} \quad (22)$$

2.3 Boundary Conditions

These are given in Table 1 for the solid and hollow cylindrical cases. Here $\bar{r} = 0$ along the centre line of the pellet, and $\bar{z} = 0$ at a distance L normal from the top of the pellet. For 1-D systems, the selected boundary conditions were equivalent to those of equations (23) and (24).

Table 1. Boundary conditions for solid and hollow cylinder systems. Outer wall boundary conditions are common to both cases.

Outer wall Boundary	Inner Boundary (Solid Cylinder)	Inner Boundaries (Hollow Cylinder)	
$\bar{C}_i = 1$ at $\bar{r} = 1$	$\frac{\partial \bar{C}_i}{\partial \bar{r}} = 0$ at $\bar{r} = 0$	$\bar{C}_i = 1$ at $\bar{r} = r_{in}$	(23)
$\bar{T} = 1$ at $\bar{r} = 1$	$\frac{\partial \bar{T}}{\partial \bar{r}} = 0$ at $\bar{r} = 0$	$\bar{T}_i = 1$ at $\bar{r} = r_{in}$	(24)
$\bar{C}_i = 1$ at $\bar{z} = 1$	$\frac{\partial \bar{C}_i}{\partial \bar{z}} = 0$ at $\bar{z} = 0$	$\frac{\partial \bar{C}_i}{\partial \bar{z}} = 0$ at $\bar{z} = 0$	(25)
$\bar{T} = 1$ at $\bar{z} = 1$	$\frac{\partial \bar{T}}{\partial \bar{z}} = 0$ at $\bar{z} = 0$	$\frac{\partial \bar{T}}{\partial \bar{z}} = 0$ at $\bar{z} = 0$	(26)

2.4 Diffusivity

The published literature concerned with mass transport phenomena in Fischer-Tropsch wax has taken a variety of approaches, utilising empirical models to quantify the diffusivity of CO and H_2 within the wax, *e.g.* Wilke-Chang correlation or Rough Hard Sphere model. A selection of commonly-applied diffusivity models is presented in Table 2, representing correlations used to determine the binary diffusivities D_{12} of H_2 and CO in Fischer-Tropsch

wax. The equation of Akgerman (1984) is based on the rough hard sphere model, with the terms T, $\overline{V}$, $\overline{V_0}$, M_1, M_2, σ_1 and σ_2 representing the temperature [K], the molar volumes of the solute, the molar volume of the solvent, the molecular mass of solute [g/mol], the molecular mass of solvent [g/mol] and the hard sphere diameters [Å] of the solute and solvent respectively. The Wilke-Chang equation is based on hydrodynamic theory, with the symbols φ, M_2, μ and v_m representing the association parameter [dimensionless, 1.0 for alkanes], solvent molecular mass [g/mol], the viscosity of the solvent [cP] and the molar volume of the solute at its normal boiling point [cm^3/gmol]. The frequently-cited correlation by Erkey *et al.* (1990) is a republished version of the Akgerman (1984) equation.

The core difficulty is identifying a model which yields accurate diffusion values within the range of interest. Akgerman (1984) noted that older models are often extrapolated far beyond their validated range, particularly for diffusion coefficients at high temperature. In their comparison of models, Sehabiague (2014) examined the Wilke-Chang and Erkey models across a temperature range of 350-550 K, reporting that the Wilke-Chang model consistently underestimated the diffusivity of both H_2 and CO for SASOL wax. Akgerman (1984) similarly reported Wilke-Chang diffusivities to underestimate the diffusivity of H_2 within heavy *n*-paraffin solvents.

Here, the binary diffusivity was calculated using the correlation of Akgerman (1984). Whilst previous reaction-diffusion models have employed the empirical diffusivity of Akgerman (1987), that equation is only suitable to determine diffusivities in *n*-$C_{28}H_{58}$. Rodden *et al.* (1988) compared the rough hard sphere theory to experimental diffusion results obtained in eicosane at elevated pressure (1.38 MPa) and temperatures (100-260°C), concluding that the hard sphere model of Akgerman (1984) could correctly represent the measurements.

The diffusivity of a species through a porous medium was accounted for using an effective diffusivity, estimated using the geometrical and structural properties of the pellet:

$$D_{eff} = D_{bulk}\frac{\varepsilon}{\tau} \tag{31}$$

where τ is the tortuosity factor, and ε the voidage.

Table 2. Correlations used in the modelling of diffusion in Fischer-Tropsch waxes.

Equation	**Application of model**

Akgerman (1984) (27) $$D_{12}\,[\mathrm{cm^2/s}] = \frac{0.945\sqrt{T}(\overline{V} - B\overline{V_0})}{(M_1)^{0.239}(M_2)^{0.781}(\sigma_1\sigma_2)^{1.134}}$$ Erkey *et al.* (1990) $$D_{12}\,[\mathrm{m^2/s}] = \frac{94.5\times10^{-9}\sqrt{T}}{(M_1)^{0.239}(M_2)^{0.781}(\sigma_1\sigma_2)^{1.134}}\left[\overline{V}_2 - \left(1.206 + 0.0632\frac{\sigma_1}{\sigma_2}\right)\frac{N_A\sigma_2^3}{\sqrt{2}}\right]$$	Trickle bed FT reactor model: Brunner *et al.* (2015) Iron based Fischer-Tropsch reaction simulation: Hallac *et al.* (2015) Fischer-Tropsch Slurry Bubble Column Model: Sehabiague (2012)
Wilke and Chang (1955) (28) $$D_{12} = \frac{7.4\times10^{-8}\sqrt{(\varphi M_2)}T}{\mu(v_m)^{0.6}}$$	Wax diffusivity in a fixed bed model: Jess and Kern (2009) Damköhler number calculation: Madon and Iglesia (1994) Monolith loop reactor: DeDeugd *et al.* (2003)
Akgerman (1987) (n-$C_{28}H_{58}$ solvent only) $$D_{CO} = 5.584\times10^{-7}\exp\left(-\frac{1786.29}{T}\right)$$ (29) $$D_{H_2} = 1.085\times10^{-6}\exp\left(-\frac{1613.65}{T}\right)$$ (30)	1-D Spherical Pellet models: Wang *et al* (2001), Vervloet *et al.* (2012),

	Gardezi and Joseph (2015) Tubular Reactor Simulation: Kaskes *et al.* (2016)

The concentrations of the reactants within the Fischer-Tropsch wax were assumed to be dilute, and thus the effective diffusivity was assumed to be dependent only on the properties of the wax and the voidage and tortuosity of the catalyst support. The assumption that the diffusivity of the reactants is influenced only by the properties of the wax is necessary to simplify the system, since a concentration-dependent diffusivity would require the simulation of hundreds of components and the vapour liquid equilibrium of poorly characterised heavy hydrocarbons. To date, all pellet models have employed this simplifying assumption.

2.5 Solubility of CO and H_2 in Fischer-Tropsch Wax

Owing to the industrial application of Fischer-Tropsch slurry phase reactors, a significant body of solubility information exists for CO and H_2 in Fischer-Tropsch products, with the differing solubility of H_2 and CO acknowledged as having a significant influence on the observed activity and product selectivity (Shi and Davis, 2005). For a sparingly-soluble gas, a Henry's law approximation is appropriate, such that

$$P_i = H_i y_i \tag{32}$$

where P_i is the partial pressure and y_i is the mole fraction of species i in the solvent. The required Henry constants, H_i, were determined using the correlations developed by Marano and Holder (1997a). The Marano and Holder (1997a) model was developed from fitting experimental solubilities and has been extensively applied in the modelling of one-dimensional Fischer-Tropsch pellets, with both Vervloet *et al.* (2012) and Becker *et al.* (2016) adopting the method to determine their boundary conditions. Since the Marano and Holder (1997a) correlation was developed specifically for the solubility of CO, H_2 and other light gases from solubility results over a range of carbon numbers (16-36) and temperatures (300-553 K), it is expected the correlation should be as accurate as more complicated equation of state models at the required modelling conditions.

The Fischer-Tropsch wax density was determined using an empirical correlation developed by Marano and Holder (1997b). Their correlation, based on experimental results for FT waxes, was used to predict the liquid molar volume as a function of carbon number, with

the value transformed into mass density using the mean molecular mass of the paraffin.

2.6 Kinetics and Selectivity

The intrinsic kinetics of the Fischer-Tropsch reaction were modelled using the expression proposed by Yates and Satterfield (1991), *viz*.

$$r_{CO+H_2} = \frac{Ae^{-\frac{E_A}{R_{Gas}T}} P_{CO} P_{H_2}}{\left(1 + Be^{-\frac{E_B}{R_{Gas}T}} P_{CO}\right)^2} \tag{33}$$

The parameters A, B and activation energies were calculated for a liquid slurry reactor by Maretto and Krishna (1999) and are listed in Table 3. The rate of CO consumption was determined by dividing the rate of CO+H_2 consumption by the H_2 to CO usage ratio + 1 (~3.1). The pressure terms were transformed to liquid-phase reactant concentrations by applying Henry's law in the same manner as Vervloet *et al.* (2012) and Gardezi and Joseph (2015).

Table 3. Parameters for equation obtained by Maretto and Krishna (1999)

A [mol s^{-1} g^{-1} bar^{-2}]	B [bar^{-1}]	E_A [kJ mol^{-1}]	E_B [kJ mol^{-1}]
8.853	2.226	37	69

As noted earlier, the selectivity of the reaction is determined by the temperature and the ratio of hydrogen to carbon monoxide. The model of Vervloet *et al.* (2012), equation (34), was adopted to determine how the selectivity was influenced by hollow cylinder size and cobalt distribution. Vervloet *et al.* (2012) developed the model by fitting their equation to the published results on selectivity of de Deugd *et al.* (2003).

$$\alpha = \frac{1}{1 + k_S \left(\frac{C_{H_2}}{C_{CO}}\right)^{\sigma} \exp\left(\frac{E_S}{R_{Gas}}\left(\frac{1}{493.15} - \frac{1}{T}\right)\right)} \tag{34}$$

Equation (34) determines the chain growth parameter (α) at a point within the pellet where C_{H_2} and C_{CO} represent the wax phase concentrations in mol/m^3 of hydrogen and carbon monoxide respectively. The dimensionless parameter k_S represents the ratio of the propagation and the termination reaction rate constants and E_S represents the effective activation energy of k_S. The values of these parameters were obtained from Vervloet *et al.* (2012) with k_S = 56.7×10^{-3}, E_S = 120 kJ/mol and σ =1.76.

2.7 Properties of the Catalyst Support

These are given in Table 4. The average thermal conductivity was determined using the Landauer equation, as recommended by Smith *et al.* (2013). The base thermal conductivities were assumed to be 1.3 W/m K for the support skeleton and 0.14 W/m K for the Fischer-Tropsch wax within the pores. The conductivity selected for the support is typical of silica, a commonly used support in the Fischer-Tropsch reaction, with the Fischer-Tropsch wax thermal conductivity calculated from the results of Marano and Holder (1997c). The influence of the impregnated metal on the thermal conductivity of the support was neglected. The porosity and tortuosity of the pellet were assumed to be 0.5 and 2 respectively, consistent with supported Fischer-Tropsch catalysts examined in the literature.

Table 4. Catalyst physical properties used in the model.

Catalyst Physical Properties	
Density of particle (inclusive of voids) [kg/m^3]	1000
Porosity of pellet [-]	0.5
Tortuosity of pellet [-]	2
Heat Transfer Physical Properties	
Mean thermal conductivity of pellet [W/m K]	0.53

3 Method of Solution

The equations were solved using orthogonal collocation on finite elements method (OCFE), (Carey and Finlayson 1975). Details are given in the Appendix. The accurate determination of the concentration profiles and the associated effectiveness factor and selectivity required a fine mesh of collocation points, such that the solution developed was independent of the mesh spacing, and thus representative of the modelled behaviour, rather than artefacts of the numerical methods. A balance between the number of elements, and thus total number of collocation points, must be found to minimise the computation time and memory usage, whilst maintaining an accurate solution. The number of collocation points per element was maintained at 5, with the number of elements varied to analyse the solution's sensitivity to the mesh spacing. The concentration gradients and effectiveness factors were found to be invariant to increasing element number above a 12×12 grid. The element sizes were refined to increase the number of elements in the regions of sharpest concentration gradients. For the 2-D simulations displayed in the following sections, a larger grid (30×30) was used to ensure accuracy across the full range of operating conditions and boundary conditions. A

typical simulation with 900 elements lasted between 2 and 5 minutes (Intel *i*3 2.2 GHz processor, 8 GB RAM), depending on the boundary condition.

The two-dimensional model was validated by comparing its predictions to analytical solutions for 1-D systems using simple first-order kinetics. The concentration profiles in the axial and radial dimensions were examined for pellets of large radii, such that the axial concentration profile was unaffected by radial contributions, and similarly at large pellet length, such that the radial profiles were unaffected by pellet length. Each profile was found to be in agreement with the analytical solution for a first order reaction in the respective 1-D cases (slab and infinite cylinder). With respect to the effectiveness factors determined for a finite hollow cylinder, the model was run using first-order single reactant kinetics and compared to the analytical solution presented by Wijngaarden *et al.* (1998), with good agreement being obtained.

4 Results

4.1 Effectiveness Factors for Solid Particles

In order to compare catalyst pellets of different dimensions and forms, the generalised Thiele modulus (Φ) was defined according to the definition of Aris (1957), equation (35). The concentration of carbon monoxide was assumed to be the limiting reagent and verified to be the case for the presented simulations.

$$\Phi = \left(\frac{V_P}{S_P}\right)\sqrt{\frac{\left(-R_{CO}{}^{s}\right)}{D_{CO,eff}C_{CO}{}^{s}}} \tag{35}$$

Here, $\left(\frac{V_P}{S_P}\right)$ represents the characteristic diffusion length, defined as the catalyst particle's volume divided by its external surface area, $-R_{CO}{}^{s}$ and $C_{CO}{}^{s}$ represent the surface rate of reaction of CO and surface concentration of CO, respectively, and $D_{CO,eff}$ represents the effective diffusivity of CO within the catalyst's pores. The effectiveness factor was defined as

$$\eta = \frac{\int_0^1\int_{\bar{r}_{in}}^1 \bar{r}(\bar{r},\bar{z})\overline{R_{CO}}(\bar{r},\bar{z})d\bar{r}d\bar{z}}{\int_0^1\int_{\bar{r}_{in}}^1 \bar{r}d\bar{r}d\bar{z}} \tag{36}$$

The evaluation of effectiveness factor across the different pellet models provided a means of determining the expected error when assuming a 1-D, instead of a 2-D, shape for conditions

typically employed in the Fischer-Tropsch process (473-513 K, 10-40 bara). Figure 2 compares slab and sphere models at constant temperature and pressure and at three separate H_2/CO ratios. Both geometries exhibited effectiveness factors greater than unity at external H_2/CO ratios greater than ~1.25. Under these conditions, the lower diffusivity of CO within the wax relative to hydrogen resulted in increased intra-particle H_2/CO ratios above that of the boundary value. This increase in H_2/CO ratio causes an increased reaction rate within the particle because the inhibitory action of CO is reduced. At a H_2/CO ratio of ~1, hydrogen and carbon monoxide are both limiting, with H_2 becoming the limiting reagent below this ratio. For the conditions in Figure 2, CO remains the limiting reagent under the reaction conditions. The position of the asymptote at high Thiele modulus to which the shapes converge is a function of H_2/CO ratio. This variation is due to the expression of the generalised modulus assuming a pseudo- first order reaction in CO. However, for rate expressions of the form used by Yates and Satterfield (1991), the average reaction order with respect to CO is a function of H_2/CO ratio, and thus depends on the surface boundary condition and the extent of conversion within the pellet.

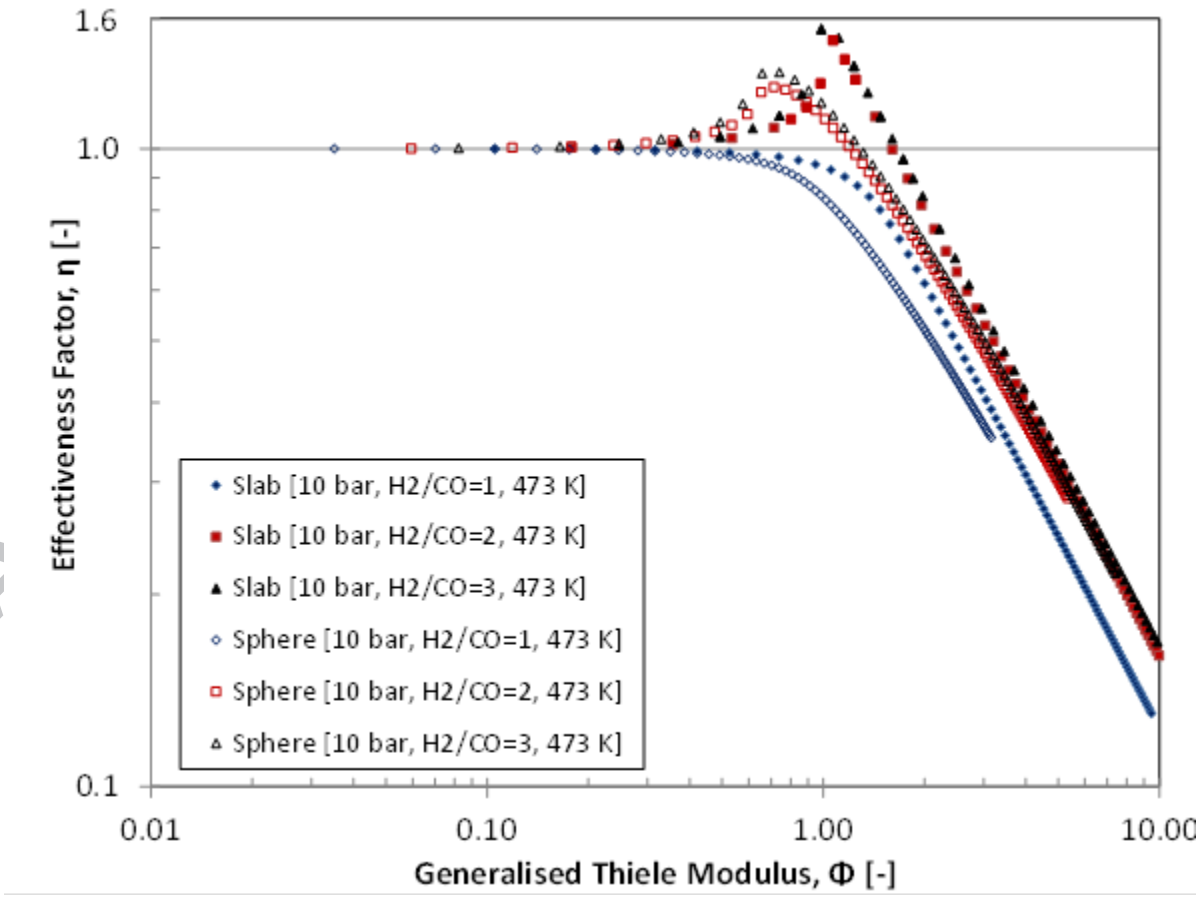

Figure 2. Effectiveness factor (η) versus generalised Thiele modulus (Φ) for sphere and slab geometry at T=473 K, P=10 bar and H_2/CO ratios of 1, 2 and 3.

The influence of the reaction pressure and temperature were characterised for spherical geometry in Figure 3. By increasing the pressure, the concentration of CO and H_2 in the Fischer-Tropsch wax increased according to Henry's law. The surface rate of reaction however increased to a lesser extent due to the inhibitory influence of CO. Hence, an increase in pressure increases the thickness of the reaction zone, and thus reduces the fraction of 'inert' core within the pellet. The changes in the peak effectiveness factor are due to the form of the kinetics. At high CO concentrations, the rate is almost proportional to H_2/CO ratio. However at low CO concentrations, the magnitude of the rate is proportional to the H_2 concentration, and thus higher H_2 concentrations at the boundary result in greater rates within the pellet as the CO concentration decreases.

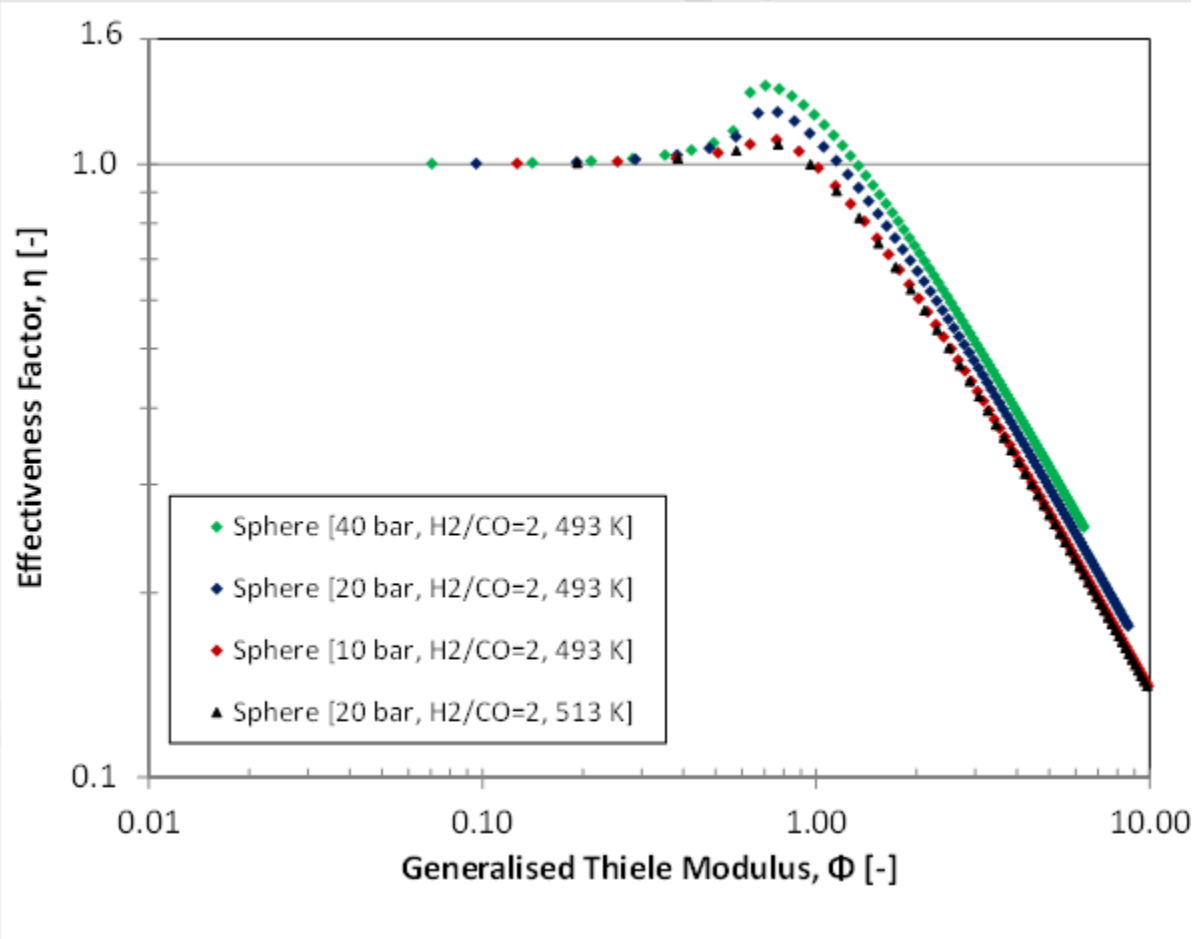

Figure 3. Effectiveness factor (η) versus generalised Thiele modulus (Φ) for a sphere under different reaction pressures and temperatures.

An increase in the temperature of reaction has been reported in the literature to increase the methane selectivity. The Henry constant for both CO and H_2 has been shown

experimentally to decrease with increase in temperature, with the correlation of Marano and Holder (1997c) accounting for this behaviour. Similarly, the effect of decreases in the density of the wax with increased temperature have also been accounted for by Marano and Holder (1997b). Overall, the molar concentration of hydrogen and carbon monoxide within the Fischer-Tropsch wax in fact increases with temperature by 1.14% for H_2 and 4.58% for CO between 220°C and 240°C. The form of the effectiveness factor curve appears to change with temperature, with the 513 K curve peaking lower than that of the 493 K curve. The increased solubility of the reactants within the wax phase is accompanied by an increase in methane selectivity, which in turn results in a higher rate of hydrogen consumption. This increased H_2 consumption and increased relative CO solubility appear to result in the reduced magnitude of the peak effectiveness factor in the η-Φ plot.

The peaking of the effectiveness factor due to the increased intra-particle H_2/CO ratio is also accompanied by a decline in the chain growth parameter, α, and thus an increased methane selectivity. The influence of mass transport on the selectivity is further discussed in Section 4.4.

4.2 Effectiveness Factors for Hollow Cylindrical Pellets

The patent literature concerning hollow cylindrical pellets suggests dimensional bounds for industrial hollow pellets, with outer radii, r_{out}, between 0.5 and 20 mm and ratios of inner (r_{in}) to outer radii between 0.1 and 0.7. A selection of patents related to hollow cylinders and their dimensional ranges are given in Table 1. It is clear that the dimensions of hollow cylinders may vary significantly in both diameter, and aspect ratio. From the patent literature, it appears that the length of the pellet varies from 0.5 up to 3.75 times the external radius. To examine the changes in selectivity and activity with the changes in the dimensions of the pellet, the performance of the catalyst was analysed over the range of conditions summarised in Table 2.

Table 1. Dimensions of hollow cylindrical pellets in patent literature. A † indicates a value was not explicitly stated.

Diameter [mm]		Length [mm]	Notes	Reference
Internal	External			
3-8	5-12	3-12		US Patent 4382021
1-3	3-6	3-6	1.0-1.5 mm wall thickness	US Patent 4366093
1.8	5	5		US Patent 4740644
1-2	4-6	†	Length of 1.75 to 3.75 external diameter.	US Patent 5166120

2-2.8	4.0-7.0	6.1-6.9	r_{in}/r_{out} ratio of 0.4-0.5	European Patent 1053789 A1
†	0.5-5	†	r_{in}/r_{out} = 0.1-0.4.	European Patent 0428223
†	3-20	†	r_{in}/r_{out} = 0.1-0.7 Length of 0.2 to 2 times external diameter.	US Patent 4656157A

Table 2. Simulation conditions for 2-D hollow cylinder model using Yates and Satterfield (1991) kinetics.

Temperature [K]	473, 493, 513
Pressure [bara]	10, 20, 40
H_2/CO ratio [-]	1, 2, 3
Outer radii (r_{out}) [mm]	Variable
Length [mm]	Variable
r_{in}/r_{out} radii ratio, μ [-]	0.2, 0.4, 0.5, 0.6, 0.8

The effectiveness factors for the 2-D hollow cylinder model are shown in Figure 4 relative to those of the 1-D slab, 1-D hollow cylinder and sphere models. The points for the 2-D hollow cylinder encompass radius ratios (μ) between 0.2 and 0.8, with length/diameter ratios (λ) between 0.5 and 3 and outer radii of 1.5, 2.0 and 3.0 mm. The values of the hollow cylinder effectiveness factor lie between those of the slab and the sphere at generalised Thiele moduli below ~0.75 and above ~1.15. Between these values, the predicted effectiveness factor is greater than both, with the peak values transitioning between that of a sphere and of a slab.

It is clear that the difference between the 2-D hollow cylinder and a 1-D slab or sphere analogue can be significant, the effectiveness factor being over- or underestimated by the 1-D analogue depending on the value of the generalised Thiele modulus. The evaluation of the effectiveness factor for the 1-D hollow cylinder demonstrates that it is reasonably approximated by a slab of analogous V_p/S_p.

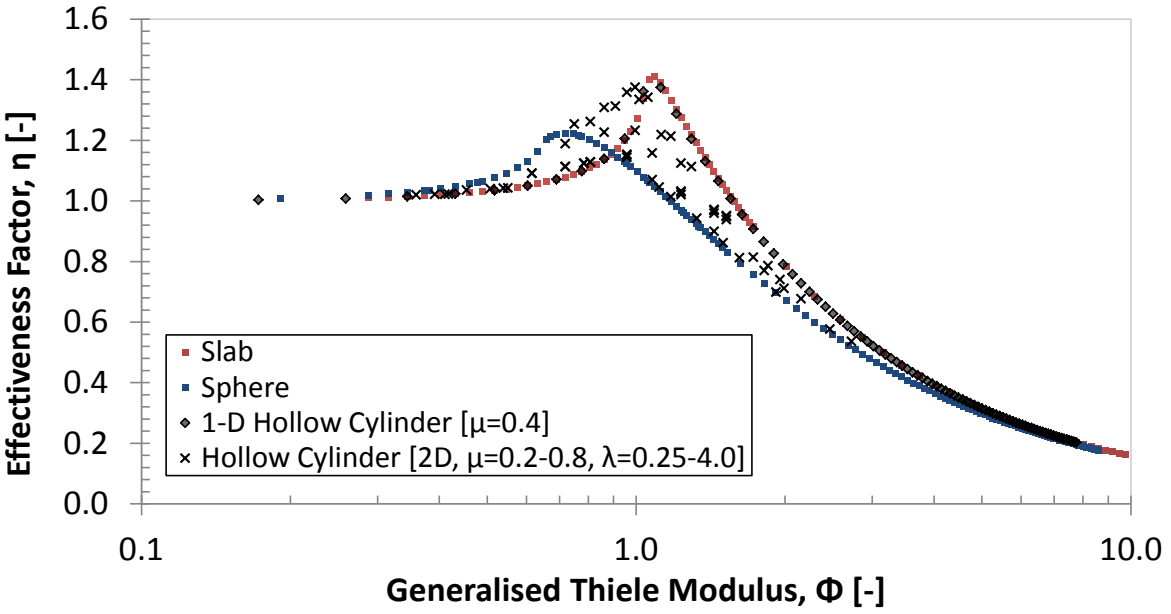

Figure 4. Effectiveness factor *versus* Thiele modulus for the 2-D hollow cylinder, 1-D hollow cylinder, slab and sphere shapes. Simulated reaction conditions of 493 K, 20 bara, $H_2/CO = 2$.

Mandic *et al.* (2017) compared the behaviour of 1-D cylinders, slabs and spheres for the Fischer-Tropsch process, reporting that the hollow cylinder provided an improved effectiveness factor relative to a slab and sphere of similar length scale. However the comparison made in their study compared hollow cylinders and slab of the same thickness, and thus different V_p/S_p ratios, since the infinite hollow cylinder has two faces exposed to the reactant gases, rather than the single face in their 1-D slab model.

Figure 5 compares the differences between the assumption of a 1-D cylindrical geometry and the 2-D geometry for the hollow cylinder. Using the generalised Thiele modulus, defined by equation (35), the effectiveness factors calculated for a 1-D hollow cylinder almost overlap for radius ratios (μ) of 0.4 and 0.8. However, it is clear that for practical hollow cylindrical pellets that the assumption of 1-D geometry may lead to significant error. The effectiveness factors for the 1-D and 2-D geometry pellets trend towards the same value at Thiele moduli above 3. However, between Thiele moduli of ~0.6 and ~2.5, differences up to ~32% in the estimated effectiveness factor are apparent for intermediate aspect ratios.

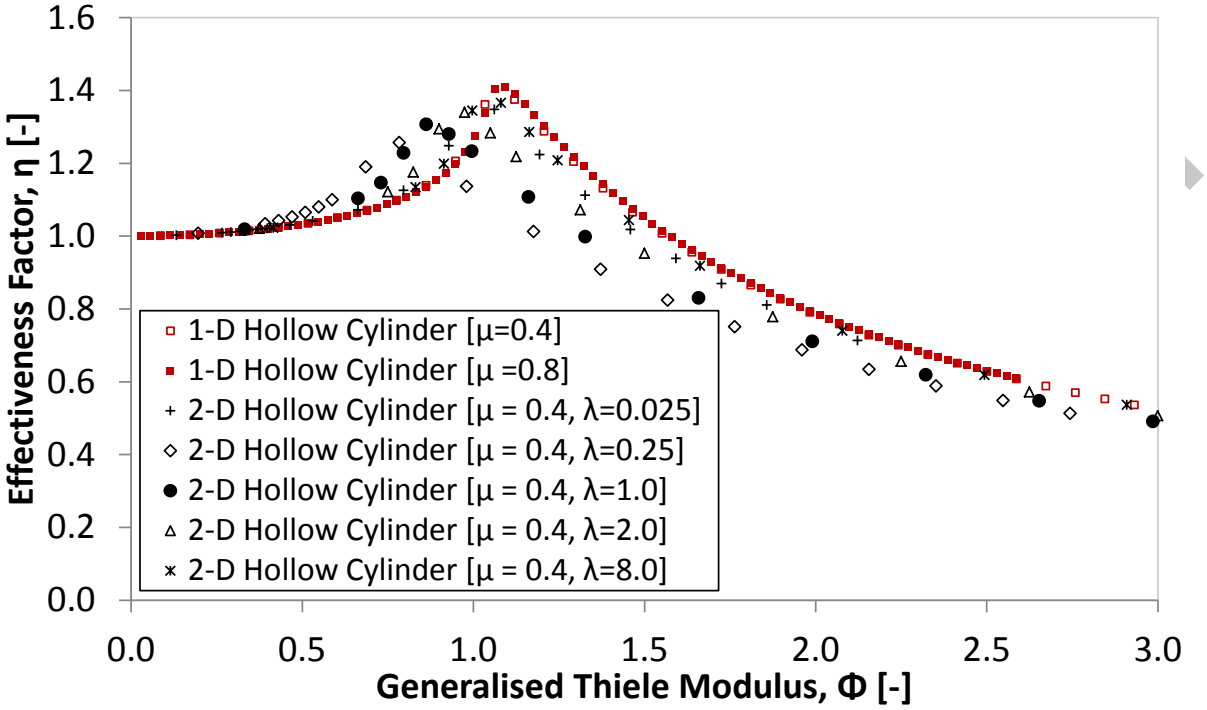

Figure 5. Effectiveness factor *versus* Thiele modulus for the hollow cylinder, slab and sphere shapes for 493 K, 20 bara, H_2/CO ratio 2.

The influence of aspect ratio (λ), defined as length divided by the outer diameter, is clearly demonstrated in Figure 5. At both high and low aspect ratios the behaviour trends towards that of a slab/infinite cylinder. In the case of hollow cylinders of practicable aspect ratios (~1-2), the position of the peak in effectiveness factor is shifted to lower Thiele moduli and shows a lower magnitude. The difference in hollow cylinder effectiveness factor in terms of $\eta_{1D}/\eta_{2D,\lambda=1}$ ranges from -18% to 13% under the reaction conditions examined. The greatest deviation from the 1-D hollow cylinder model occurs where the pellet length is comparable to its radial thickness, $(1-\mu)r_{out}$. Under these conditions the ring-form catalyst behaviour would be more closely approximated by a sphere model.

For evaluating pellets in fixed-bed reactor models, the best means of comparison might be equivalent catalyst mass. In order to compare catalysts of similar mass, a series of equivalent (solid) volume catalysts were evaluated using the 2-D hollow cylinder model. Effectiveness factors for a hollow cylindrical, solid cylindrical and spherical particle at 5 equivalent sphere diameters are given in Table 3.

Table 3. Comparison of effectiveness factors at set sphere equivalent diameter (10 bar, 493 K, Yates and Satterfield (1991) kinetics).

d_{SE} [mm]	$\eta_{Hollow,2D}$† [-]	$\eta_{Hollow,1D}$† [-]	$\eta_{Cylinder}$† [-]	η_{Sphere} [-]	$\eta_{Sphere,Brunner}$ [Equation (37)]
0.5	1.00	1.01	1.01	1.01	0.98
1.0	1.01	1.08	1.05	1.08	0.94
2.0	1.06	0.85	0.95	0.86	0.80
3.0	1.11	0.61	0.72	0.63	0.65
5.0	0.73	0.38	0.48	0.41	0.44

† Aspect ratio of 2, Inner Radius/Outer Radius = 0.4.

It can be seen that the 2-D hollow cylinder shows the best performance for a given mass of catalyst material in comparison to the other shapes due to its greater surface area per unit volume. The 1-D hollow cylinder model predicts particularly poor performance due to the neglect of the ends of the particle, with the equivalent volume comparison yielding a larger V_P/S_P ratio than the 2-D model.

4.3 Comparison with Simplified Models for Effectiveness Factor

Fixed-bed reactor studies often require simplified models to evaluate catalyst effectiveness factor without excessive computation. In their model of a 1-D fixed bed, Brunner *et al.* (2015) compared uniformly active spheres, cylinders, trilobes and hollow cylinders on the basis of equivalent catalyst masses. In order to characterise the catalyst's effectiveness factor, the authors employed an n^{th} order Thiele modulus description. This approach, originally derived by Bischoff (1965) for a slab, consisted of calculating the catalyst effectiveness factors using equations (37) and (38).

$$\Phi_{n\,th} = L' \sqrt{\frac{\left(-R_{CO}{}^{s}\right)(n+1)\left(C_{CO}{}^{s}\right)^{n}}{2D_{CO,eff}C_{CO}{}^{s}}} \tag{37}$$

$$\eta = \frac{\tanh\left(\Phi\right)}{\Phi} \tag{38}$$

Here L' is the diffusion length and n is a modifier to approximate non-first order behaviour, taken as -0.1 by Brunner *et al.* (2015) for their kinetics.

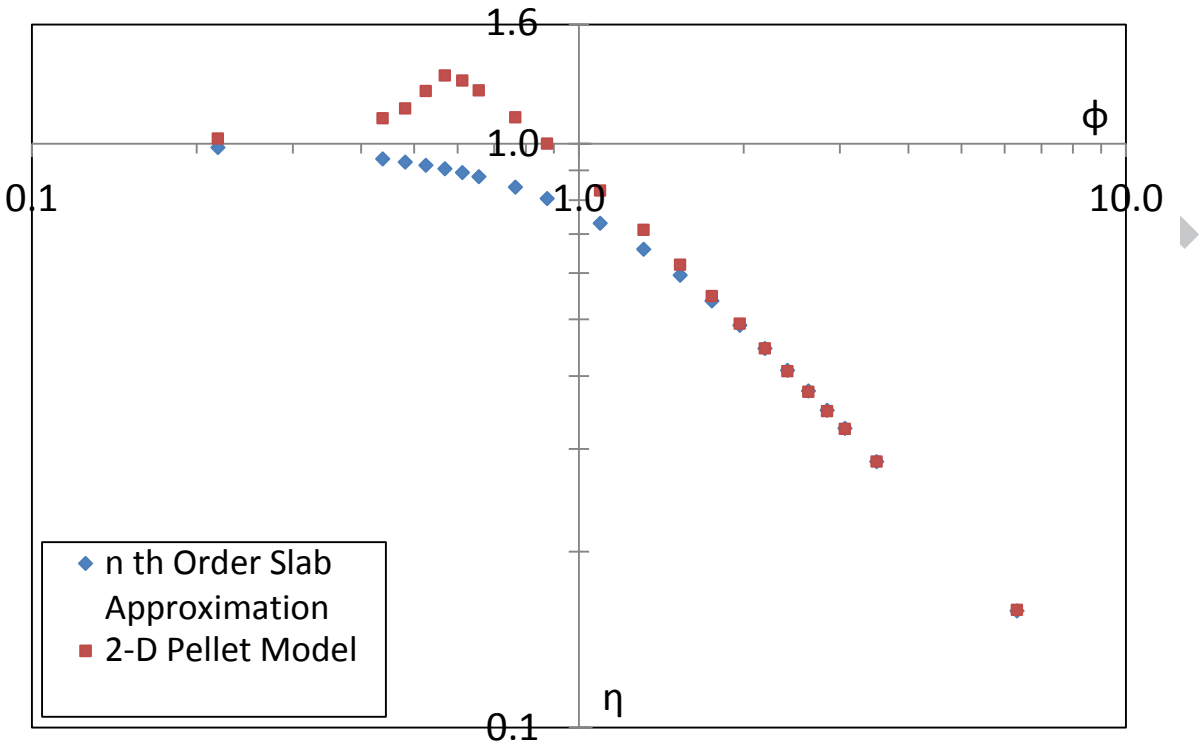

Figure 6. Comparison of the 2-D Hollow Cylinder against 1-D n^{th} order slab approximation for T = 493 K, P = 20 bar, H_2/CO ratio = 2, μ = 0.4, λ = 1.

The n^{th} order Thiele method was compared with the 2-D hollow pellet model to evaluate the differences in effectiveness factor between the methods, as shown in Figure 6 for $\Phi_{n^{th}}$ values between ~0.2 and ~7. For the Yates and Satterfield (1991) kinetics under the considered conditions, n = -0.18 was found to provide the best agreement at high values of Thiele modulus. The n^{th} order slab approximation gives a reasonable approximation at high and low values of Thiele modulus of the kinetic behaviour for Langmuir-Hinshelwood expressions of the Yates and Satterfield form, as seen in Figure 6. The degree of error in the effectiveness factor for the sphere varies across the equivalent pellet volumes, with the greatest error occurring where the predicted effectiveness factor is greater than 1. Significant differences in effectiveness factor between the n^{th} order slab model and the 2-D hollow pellet model can be seen for values of n^{th} order Thiele modulus between ~0.5 and ~1.5. It appears that for pellet effectiveness factors > 0.6, the magnitude of error between the models may exceed 5%, with the greatest error reaching 30.8% based on $\eta_{n^{th}}/\eta_{2D}$.

4.4 Evaluation of α for Different Geometries

The alpha model of Vervloet *et al.* (2012) was used to examine the influence of the pellet shape on selectivity towards higher value hydrocarbons. The reaction-weighted average

of the chain growth (α) parameter for a hollow cylinder was determined to evaluate the performance of the 2-D pellet using the integral in equation (39). Analogous reaction weighted integrals for slab, sphere and 1-D hollow cylinder geometries, equations (40)-(42) were also calculated for the purpose of comparison.

$$\alpha_{avg,\,2D\,Cylinder} = \frac{\int_0^1 \int_{\bar{r}_{in}}^1 \bar{r} \propto (\bar{r},\bar{z})\overline{R_{CO}}(\bar{r},\bar{z})d\bar{r}d\bar{z}}{\int_0^1 \int_{\bar{r}_{in}}^1 \overline{rR_{CO}}(\bar{r},\bar{z})d\bar{r}d\bar{z}} \tag{39}$$

$$\alpha_{avg,\,Slab} = \frac{\int_0^1 \propto (\bar{z})\overline{R_{CO}}(\bar{z})d\bar{z}}{\int_0^1 \overline{R_{CO}}(\bar{z})d\bar{z}} \tag{40}$$

$$\alpha_{avg,\,Sphere} = \frac{\int_0^1 \bar{r}^2 \propto (\bar{r})\overline{R_{CO}}(\bar{r})d\bar{r}}{\int_0^1 \bar{r}^2\overline{R_{CO}}(\bar{r})d\bar{r}} \tag{41}$$

$$\alpha_{avg,\,1D\,Cylinder} = \frac{\int_{\bar{r}_{in}}^1 \bar{r} \propto (\bar{r},\bar{z})\overline{R_{CO}}(\bar{r},\bar{z})d\bar{r}}{\int_{\bar{r}_{in}}^1 \overline{rR_{CO}}(\bar{r},\bar{z})d\bar{r}} \tag{42}$$

Figure 7 compares the reaction-weighted α for slab, sphere and 2-D hollow cylinders. The α values for the different geometries show a similar behaviour to the effectiveness factor plots. At low values of Φ, below 0.5, the selectivity essentially equals that at surface conditions. Above this value, the selectivity begins to decrease due to increasing intra-particle mass transfer resistances. The intra-particle ratios of H_2 : CO increase, leading to a reduction in the overall alpha. As Φ further increases, the α value tends to a steady average.

The selectivity for the 2-D hollow cylinder is bounded by the behaviour of the sphere below Φ= 0.75 and above Φ= 1.15, with the hollow cylinder displaying the lowest α values in the transition region. The lower average α values are coincident with the Thiele modulus range in which the effectiveness factor peaks. Significant differences between the average α parameter are apparent at a fixed Thiele modulus, with a maximum difference of ~32% between the hollow cylinder and analogous slab at fixed Thiele modulus.

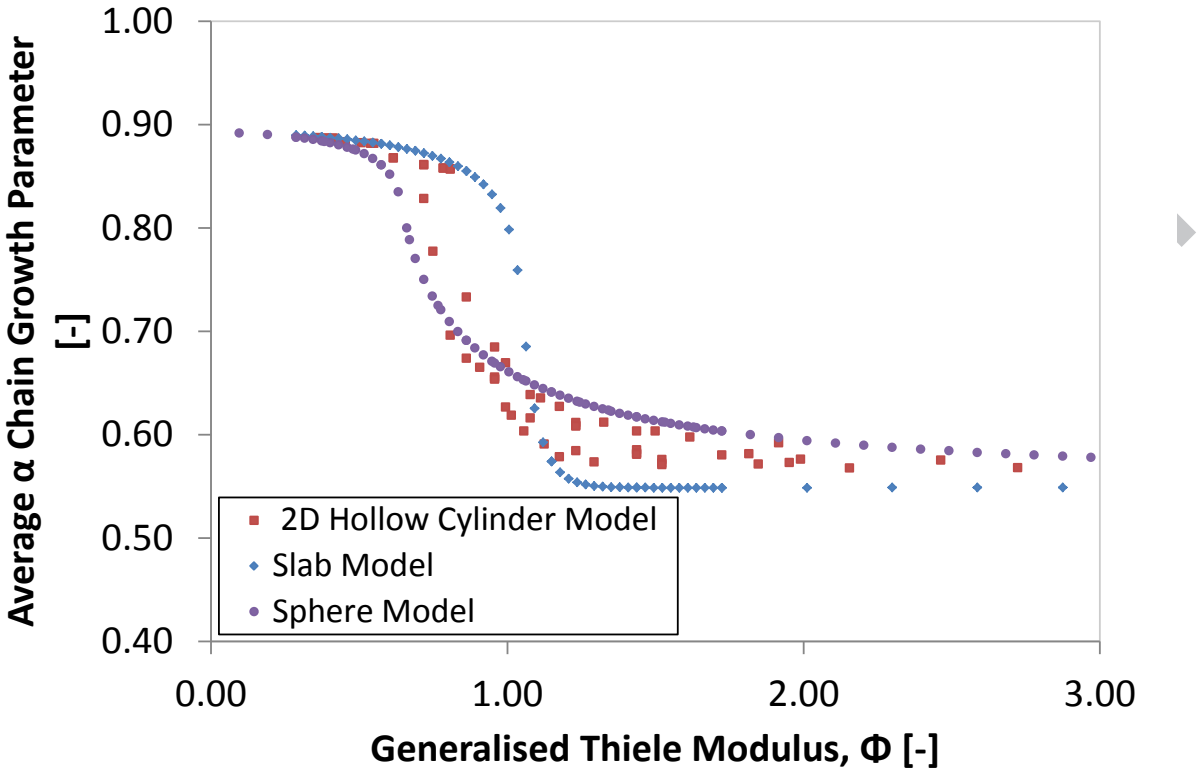

Figure 7. Comparison reaction-weighted chain growth parameter for sphere, slab and 2D hollow cylinder models (20 bar, 493 K, H_2/CO=2). For the hollow cylinder, r_{out} = 1.5, 2.0, 3.0 mm, μ = 0.2-0.8, λ = 0.25-3.

The influence of aspect ratio on the plot of chain growth parameter *versus* the generalised Thiele modulus was explored (results not shown). It was found that the selectivity of the 2-D hollow cylinder shifts between slab behaviour (or 1-D hollow cylinder) and sphere behaviour. The hollow cylinder displayed slab-like behaviour at both high (1-D cylinder) and low aspect (flat disc) ratio ($\lambda=L/D_{out}$), with varying degrees of intermediate behaviour between these two limits. The greatest deviation from the slab behaviour occurred as the length of the hollow cylinder tended to values $\approx (1-\mu)r_{out,}$ and thus having a square toroidal shape. Under these conditions, the behaviour tended towards that of a sphere.

Table 4 shows reaction-weighted average alpha parameters for solid (λ = 2) and hollow (μ = 0.4, λ = 2) cylinders at equivalent volumes. The sphere has the lowest α value, and thus the highest selectivity towards undesirable methane production. As the volume of the pellet increases, mass transfer increases, leading to higher intra-particle H_2/CO ratios, and thus greater methane selectivity. The hollow cylinder provides a greater efficiency in use of catalyst mass. This trend mirrors that noted for the effectiveness factor, with the lowered diffusion lengths for the solid and hollow cylinders relative to the sphere yielding reduced mass transfer

limitations, and thus less significant changes to the intra-particle H_2/CO ratio.

Table 4 Comparison of reaction-weighted selectivities at fixed equivalent sphere diameters (d_{SE})

d_{SE} [mm]	Reaction-Weighted Selectivity		
	Sphere	Solid Cylinder	Hollow Cylinder
1.36	0.81	0.87	0.88
3.00	0.62	0.64	0.84
3.54	0.60	0.62	0.64
3.80	0.60	0.61	0.60
5.44	0.58	0.58	0.57

The decline in the selectivity commences at a Thiele modulus of ~0.5. This corresponds to the point at which the effectiveness factor begins to rise. Hence, catalyst operating at the peak effectiveness factor will display a much poorer selectivity for heavy hydrocarbons than a kinetically controlled system. This behaviour is expected since the rise in effectiveness factor is due to an increase in intra-pellet H_2/CO ratio, and thus reduced inhibition by CO. The increased intra-pellet H_2/CO ratios also result in a lighter product distribution, favouring methane.

5 Discussion

The influence of shape on the observed behaviour for the Fischer Tropsch reaction depends significantly on the intrinsic kinetics. At low rates, and thus low Thiele moduli, the reaction is kinetically controlled and uninfluenced by the particle's shape. At high reaction rates, and thus high values of Φ, the reaction becomes limited to a thin surface layer in the particle, and thus depends mainly on the surface area of the particle. The model developed in this paper has demonstrated that at intermediate Φ values, the effectiveness factor and selectivity of the Fischer-Tropsch reaction can be significantly influenced by shape, and the evaluation of simpler one-dimensional models has highlighted the cases where the catalyst performance is insufficiently described.

The form of the Langmuir-Hinshelwood kinetics, in combination with the selectivity equation of Vervloet *et al.* (2012), gives rise to effectiveness factors > 1, with differences between the particle shapes most prominent between generalised Thiele moduli of ~0.5 and ~1.5. The intrinsic kinetics available in the literature for the Fischer-Tropsch process have been

reported over a significant range, with rates of CO consumption spanning orders of magnitude from 0.1 to 10s of mmol/kg_{cat} s, *e.g.* Keyser *et al.* (2000), Atashi *et al.* (2012), Lögdberg *et al.* (2011). The magnitude of the value depends on the catalyst formulation, conversion, pressure, H_2/CO ratio and with a significant dependence on temperature. The Yates and Satterfield (1991) kinetic model selected yielded intrinsic rates consistent within this range, with rates of ~0.2 - 5.3 mmol/kg_{cat} s for the modelled conditions.

Because the reaction is exothermic, operation of catalysts with the highest intrinsic activities may lead to undesirable temperature gradients and the potential for runaway reaction. Indeed, the fixed-bed modelling study of Jess and Kern (2009) simulated the temperature profiles within a multi-tubular reactor for 2.7 mm diameter cobalt catalyst cylinders within a 46 mm diameter tube. The authors predicted that exothermic runaway could occur where the reactor inlet and wall cooling temperatures were both 215°C, which corresponded to an intrinsic reaction rate at the inlet of ~3.2 mmol/kg_{cat} s for their kinetic model.

Here, an isothermal pellet assumption was made to reduce the computational requirements. Under the simulated conditions, the assumption was determined to be reasonable, in agreement with one-dimensional studies. The boundary conditions assumed a fixed surface and thus pellet temperature, consistent with previous modelling studies, *e.g.* Vervloet *et al.* (2012), Gardezi and Joseph (2015). Within a fixed-bed, the external temperature of a pellet will depend on its position within its bed, the diameter of the tube, the diameter of the pellet, and the heat transfer coefficients between the wall, coolant and pellets.

The model assumed that the pores are entirely and uniformly filled with wax. The wax within the pores is generated internally at the catalyst sites and it is likely that removal of long chain hydrocarbons from within the pore network will be frustrated by mass transport limitations. The assumption of filled pores has been applied in prior pellet models, with Pohlman and Jess (2016) recently investigating the degree of filling within Fischer-Tropsch pellets experimentally. Their examination of pore filling found carbon species to be deposited evenly throughout the pellet, in contrast to the core-shell approach adopted by Gardezi and Joseph (2015) to model partially filled particles. Pohlman and Jess (2016) determined the degree of filling *via* thermogravimetric analysis of used catalyst particles, reporting 100% filling at 200°C, with the degree subsequently decreasing with temperature. Pohlman and Jess (2016) found that a homogenous approach adequately described the mass transfer phenomena within partially-filled pellets, determining the effective diffusivity through a combination of gas and liquid phase diffusivities in proportions determined by the experimentally-determined

liquid filled fraction. In this paper, a fully-filled particle was assumed, and whilst this condition may not hold true under certain operating conditions, with the pore filling degree dependent on temperature, liquid composition and pore size, the work of Pohlman and Jess (2016) demonstrates that a homogenous approach can provide agreement with experimental results. Hence the conclusions on the influence of pellet shape developed within this chapter remain applicable, and may be extended to partially-filled pellets by modifying the effective diffusivity, and thus the generalised Thiele modulus.

The extent of mass transfer limitation observed within a Fischer-Tropsch pellet of practical scale (~ millimetre) depends significantly on the selected catalyst activity. By using a generalised Thiele modulus, the model developed permits evaluation of the influence of shape on the observed selectivity and effectiveness. It is evident that catalyst performance is sensitive to shape at Thiele moduli between 0.5 and 3, or effectiveness factors greater than ~0.55. Comparing different geometries at equivalent V_P/S_P, the selectivity for the hollow cylinder was noted to reach values below those for the slab or sphere geometry between Thiele values of 0.75-1.15. Despite the region indicating lower selectivity, hollow cylinders compared to spherical pellets of equivalent volume demonstrate improved selectivity, attributable to their lower V_P/S_P value at equivalent volume.

Other pellet-scale investigations have neglected the axial dimension in their considerations of hollow cylindrical pellets. However it has been demonstrated here to have a noticeable influence on catalyst performance at practical aspect ratios. Mandic *et al.* (2017) considered an infinite hollow cylinder, employing a simplified reaction scheme with fixed H_2/CO stoichiometry and modelling methane selectivity through consideration of a secondary reaction path solely for methane formation. The authors' comparison of slab, spherical egg-shell and infinite hollow cylinders at fixed thickness led them to conclude that diffusional resistance decreased in the order hollow cylinder < egg-shell sphere < slab, with the difference attributed to the changes in diffusional length ($L=V_p/S_p$). The present research has shown that the 1-D hollow cylinder model appears well approximated by the slab assumption at equivalent V_p/S_p. However, consideration of the axial dimension is necessary at aspect ratios below 8 for an inner/outer radius ratio of 0.4. The greatest deviation from slab behaviour occurred where the radial and axial length scales were comparable, with catalyst of square toroidal form behaving more similarly to the spherical particle model.

Shaped extrudates and hollow cylinders have been simulated in the literature to show superior fixed-bed performance in comparison to spherical particles in terms of both pressure drop and catalyst mass requirements. Here, the effectiveness factors and selectivities of

different geometries have been evaluated in detail at both fixed volume to surface area ratio and fixed mass. At constant catalyst mass, the hollow cylindrical pellets provide significantly greater surface area than solid cylinders or spheres of equivalent mass, and thus a reduced effective diffusion length leading to an improved effectiveness factor and selectivity.

Whilst the scope of this paper does not extend to multi-hole pellets, it has been demonstrated that the neglect of axial contributions for a simpler single-hole pellet may result in significant error under certain conditions. In order to evaluate the validity of a simplified n^{th} order effectiveness factor model, a comparison was developed between the output from the 2-D model and the analytical approach. It was found to provide reasonable agreement (within 5%) to the detailed models at Thiele moduli below 0.5 and above 2, provided the effective order of the modulus was fitted to the pellet models at high Thiele values. The use of a simplified model significantly reduces the complexity and duration of calculation. However, as shown earlier, the asymptote for the η-Φ plot shifts with reaction conditions, and thus the effective reaction order will change with conversion along the length of the reactor. Hence, assuming a constant reaction order across the length of a reactor could give significant error.

Industrially, the operation of the reactor in the region where $\eta > 1$ would be unfavourable. Despite the increased reaction rate, the changes in the intraparticle H_2/CO ratio decrease the yield of the valuable heavier products, and result in the production of greater quantities of methane. Similarly, operation at a high Thiele modulus leads to excessive methane production and inefficient utilisation of the catalyst material. In order to avoid extensive mass transport issues whilst maintaining acceptable selectivities, an egg-shell distribution needs to be adopted, as is widespread in industry. However, as with alterations to the catalyst shape, detailed consideration would be required to balance the overall catalyst and thus reactor volume with any gains in selectivity and effectiveness factor from the egg shell distribution.

6 Conclusions

A reaction-diffusion model for a 2-D hollow cylinder has been developed. The model has been analysed across a range of Thiele moduli and the extent of error in both effectiveness factor and α parameter have been quantified relative to one-dimensional sphere and slab geometries. The application of 2-D modelling was noted to result in errors between slab, sphere and 1-D hollow cylinder geometries between Thiele moduli of ~0.25 to ~3.

Effectiveness factors were bounded by those of sphere and slab above and below Thiele moduli of ~0.75 and ~1.15 respectively for the conditions examined, with the effectiveness factors exceeding those of both sphere and slab models between these moduli. Concurrently,

the α parameters between these values were lower than both those of sphere and slab geometry, and thus under these conditions hollow cylinders provide the greatest methane selectivity.

The model was evaluated against a simplified n^{th} order effectiveness factor model employed in fixed bed modelling and found to differ over the Thiele range ~0.5 to ~1.5, with the greatest errors arising where the effectiveness factor exceeded unity. The use of the simplified model further required fitting at high values of Thiele modulus in order to provide a reasonable representation of catalyst behaviour. However, the effective order of the reaction was noted to be dependent on the reaction conditions and thus selection of an appropriate reaction order represents a further source of error in fixed-bed modelling where the surface conditions of a pellet are a function of bed-length. A comparison of the hollow cylindrical pellets against spheres of equivalent volume demonstrated that the hollow cylinder provided improved fixed-bed performance, with greater effectiveness factors and selectivities due to the lowered diffusion lengths for the hollow cylindrical geometry.

Acknowledgements

R. A. H. would like to thank the EPSRC for provision of a Doctoral Training Grant.

References

Akgerman, A. 1984. Diffusivities of Synthesis Gas and Fischer-Tropsch Products in Slurry Media. Final Report. DOE Report-DOE/PC/70032-T2.

Akgerman, A. 1987. Final Report to US DOE. Contract No. DE-AC22-84PC701132.

Anderson, R. B., Seligman, B., Schultz, J.F., Kelly, R., Elliot, M.A., 1952. F-T Synthesis: Some Important Variables of the Synthesis on Iron Catalysts, Ind. Eng. Chem. 44(1), 391-397.

Aris, R., 1957. On Shape Factors for Irregular Particles-1: The Steady State Problem, Diffusion and Reaction. Chem. Eng. Sci., 6, 262-268.

Atashi, H., Mansouri, M., Hosseini, S.H., Khorram, M., Mirzaei, A.A., Karimi, M., Mansouri, G., 2012. Intrinsic kinetics of the Fischer-Tropsch synthesis over an impregnated cobalt-potassium catalyst. Korean Journal of Chemical Engineering, 29, 304-309.

Becker, H., Güttel, R., Turek, T., 2014. Optimization of Catalysts for Fischer-Tropsch Synthesis by Introduction of Transport Pores. Chemie Ingenieur Technik, 86(4), 544-549.

Becker, H., Güttel, R., Turek, T., 2016. Enhancing internal mass transport in Fischer–

Tropsch catalyst layers utilizing transport pores. Catal. Sci. Technol., 6, 275-287.

Bischoff, K.B., 1965. Effectiveness factors for general reaction rate forms. AIChE J., 11, 351-355.

Brunner, K. M., Perez, H. D., Peguin, R. P. S., Duncan, J. C., Harrison, L. D., Bartholomew, C. H., Hecker, W. C., 2015. Effects of Particle Size and Shape on the Performance of a Trickle Fixed-Bed Recycle Reactor for Fischer-Tropsch Synthesis. Ind. Eng. Chem. Res., 54, 2902-2909.

Carey, G. F., Finlayson, B. A., 1975. Orthogonal Collocation on Finite Elements. Chem. Eng. Sci., 30, 587-589.

De Deugd, R. M. Chougule, R. B. Kreutzer, M. T. Meeuse, F. M., Grievink, J., Kapteijn, F., Moulijn, J. A., 2003. Is a monolithic loop reactor a viable option for Fischer-Tropsch synthesis? Chem. Eng. Sci., 58, 583-591.

Dry, M.E., 2002. The Fischer – Tropsch process : 1950 – 2000. Catal. Today, 71, 227–241.

Erkey, C., Rodden, J. B., Akgerman, A., 1990. Diffusivities of synthesis gas and n-alkanes in Fischer-Tropsch wax. Energy & Fuels, 4, 275-276.

Gardezi, S. A., Joseph, B., 2015. Performance Characteristics of Eggshell Co/SiO2 Fischer-Tropsch Catalysts: A Modelling Study. Ind. Eng. Chem. Res., 54, 8080-8092.

Gaube, J., Klein, H.-F., 2008. Studies on the reaction mechanism of the Fischer–Tropsch synthesis on iron and cobalt. J. Molec. Catal. A: Chemical, 283 (1–2), 60–68.

Huff, G.A., Satterfield, C.N., 1984. Evidence for two chain growth probabilities on iron catalysts in the Fischer-Tropsch synthesis. J Catal., 85 (2), 370–379.

Huff, G.A., Satterfield, C.N., 1985. Liquid accumulation in catalyst pores in a Fischer-Tropsch fixed-bed reactor. Ind. Eng. Chem. Res., 24, 986–995.

Iglesia, E., Reyes, S.C. and Madon, R.J., 1991. Transport-Enhanced a-Olefin Readsorption Pathways in Ru-Catalyzed Hydrocarbon Synthesis. J. Catal., 129, 238–256.

Iglesia, E., Soled. S. L., Baumgartner, J. E., Reyes, S. C., 1995. Synthesis and catalytic properties of eggshell cobalt catalysts for the Fischer-Tropsch synthesis. Top. Catal., 2(1), 17-27.

Jess, A., Kern, C., 2009. Modeling of Multi-Tubular Reactors for Fischer-Tropsch

Synthesis. Chem. Eng. Technol., 32 (8), 1164–1175.

Kaiser, P., Pöhlmann, F., Jess, A., 2014. Intrinsic and Effective Kinetics of Cobalt-Catalyzed Fischer-Tropsch Synthesis in View of a Power-to-Liquid Process Based on Renewable Energy. Chem. Eng. Technol., 37 (6), 964–972.

Kaskes, B., Vervloet, D., Kapteijn, F., van Ommen, J. R., 2016. Numerical optimisation of a structured tubular reactor for Fischer-Tropsch synthesis. Chem. Eng. J., 283, 1465-1483.

Keyser, M.J., Everson, R.C., Espinoza, R.L., 2000. Fischer-Tropsch kinetic studies with cobalt-manganese oxide catalysts. Ind. Eng. Chem. Res., 39, 48-54.

King, D., 1978. A Fischer-Tropsch study of supported ruthenium catalysts. J. Catal., 51, 386–397.

Kuipers, E., Scheper, C., Wilson, J., Vinkenburg, I. and Oosterbeek, H., 1996. Non-ASF product distributions due to secondary reactions during Fischer-Tropsch synthesis. J. Catal., 158 (1), 288–300.

Kuipers, E.W., Vinkenburg, I.H., Oosterbeek, H., 1995. Chain Length Dependence of alpha-Olefin Readsorption in Fischer-Tropsch Synthesis. J. Catal., 152, 137–146.

Leckel, D., 2009. Diesel Production from Fischer−Tropsch: The Past, the Present, and New Concepts. Energy & Fuels, 23 (5), 2342–2358.

Madon, R., Iglesia, E., 1994. Hydrogen and CO intrapellet diffusion effects in ruthenium-catalyzed hydrocarbon synthesis. J. Catal., 149, 428–437.

Makrodimitri, Z. A., Unruh, D. J. M., Economou, I. G., 2011. Molecular simulation of diffusion of hydrogen, carbon monoxide, and water in heavy n-alkanes. J. Phys. Chem. B, 115, 1429-1439.

Mandić, M., Todić, B., Živanić, L., Nikalčević, N., Bukur, D. B., 2017. Effects of Catalyst Activity, Particle Size and Shape, and Process Conditions on Catalyst Effectiveness and Methane Selectivity for Fischer-Tropsch Reaction: A Modelling Study. Ind. Eng. Chem. Res., 56, 2733-2745.

Marano, J.J., Holder, G.D., 1997a. Characterization of Fischer-Tropsch liquids for vapor-liquid equilibria calculations. Fluid Phase Equilibria, 138, 1-21.

Marano, J. J., Holder, G.D., 1997b. Prediction of Bulk Properties of Fischer-Tropsch

Derived Liquids. Ind. Eng. Chem. Res., 36, 2409-2420.

Marano, J. J., Holder, G. D., 1997c. A General Equation for Correlating the Thermophysical Properties of n-Paraffins, n-Olefins, and Other Homologous Series. 3. Asymptotic Behaviour Correlations for Thermal and Transport Properties. Ind. Eng. Chem. Res., 36, 2399-2408.

Maretto, C. and Krishna, R., 1999. Modelling of a bubble column slurry reactor for Fischer-Tropsch synthesis. Catal. Today, 52 (2-3), 279–289.

Masuku, C., Hildebrandt, D. and Glasser, D., 2011. The role of vapour–liquid equilibrium in Fischer–Tropsch product distribution. Chem. Eng. Sci., 66 (23), 6254–6263.

Nanduri, A., Mills, P. L., 2015. A Wall-Cooled Fixed-Bed Reactor for Gas-Phase Fischer-Tropsch Synthesis. Excerpt from the Proceedings of the 2015 COMSOL Conference, Boston.

Novak, S., Madon, R.J., Suhl, H., 1981. Models of hydrocarbon product distributions in Fischer–Tropsch synthesis. I. J. Chem. Phys., 74 (11), 6083–6091.

Pohlmann, F., Jess, A., 2016. Interplay of reaction and pore diffusion during cobalt-catalyzed Fischer-Tropsch synthesis with CO_2-rich syngas. Catal. Today, 275, 172-182.

Post, M.F.M., Van't Hoog, a. C., Minderhoud, J.K., Sie, S.T., 1989. Diffusion limitations in Fischer-Tropsch catalysts. AIChE J., 35 (7), 1107–1114.

Rodden, J. B., Erkey, C., Akgerman, A., 1988. High-Temperature Diffusion, Viscosity and Density Measurements in n-Eicosane. Journal of Chemical and Engineering Data, 33(3), 344-347.

Sánchez-López, J. R. G., Martínez-Hernández, A., Hernández-Ramírez, A., 2016. Modelling of transport phenomena in fixed-bed reactors for the Fischer-Tropsch reaction; a brief literature review. Rev. Chem. Eng., 33(2), 1-33.

Sehabigue, L., 2012. Modelling, Scale-Up and Optimization of Slurry Bubble Column Reactors for Fischer-Tropsch Synthesis. PhD Thesis, University of Pittsburgh.

Shi, B., Davis, B.H., 2005. Fischer–Tropsch synthesis: The paraffin to olefin ratio as a function of carbon number. Catal. Today, 106 (1–4), 129–131.

Smith, D. S., Alzina, A., Bourret, J., Nait-Ali, B., Pennec, F., Tessier-Doyen, N., Otsu, K., Matsubara, H., Elser, P., Gonzenbach, U. T., 2013. Thermal conductivity of porous

materials. J. Mat. Res., 28(17), 2260-2272.

Snel, R., 1987. Olefins from Syngas. Catal. Rev., 29 (4), 361–445.

van der Laan, G.P., Beenackers, A.A.C.M., 1999. Kinetics and Selectivity of the Fischer–Tropsch Synthesis: A Literature Review. Catal. Rev., 41 (3&4), 255–318.

Vervloet, D., Kapteijn, F., Nijenhuis, J., van Ommen, J.R., 2012. Fischer–Tropsch reaction–diffusion in a cobalt catalyst particle: aspects of activity and selectivity for a variable chain growth probability. Catal. Sci. Technol., 2 (6), p.1221.

Wang, Y.-N., Xu, Y.-Y., Xiang, H.-W., Li, Y.-W., Zhang, B.-J., 2001. Modelling of Catalyst Pellets for Fischer−Tropsch Synthesis. Ind. Eng. Chem. Res., 40 (20), 4324–4335.

Wijngaarden, R.J., Kronberg, A., Westerturp, K.R., 1998. Industrial Catalysis Optimising Catalysts and Processes, Wiley-VCH, Weinheim.

Wilke, C. R., Chang, P., 1955. Correlation of diffusion coefficients in dilute solutions. AIChE J., 1(2), 264-270.

Yates, I.C., Satterfield, C.N., 1991. Intrinsic kinetics of the Fischer-Tropsch synthesis on a Cobalt Catalyst. Energy & Fuels, 5, 168–173.

Highlights

A 2-D model was investigated for the FT reaction for solid and hollow cylindrical Co catalyst pellets

Conditions considered where liquid hydrocarbons accumulate in the pores

Effectiveness factor exceeded that of spherical and slab geometry for Thiele moduli range 0.75 - 1.15

FT growth parameter, α, in this range was lowest with cylinders and so gave greatest CH_4 selectivity